Heliyon 8 (2022) e09120

Contents lists available at ScienceDirect

Heliyon

journal homepage: www.cell.com/heliyon

Research article

Theoretical insights into a high-efficiency Sb_2Se_3-based dual-heterojunction solar cell

Bipanko Kumar Mondal, Shaikh Khaled Mostaque, Jaker Hossain *

Solar Energy Laboratory, Department of Electrical and Electronic Engineering, University of Rajshahi, Rajshahi, 6205, Bangladesh

HIGHLIGHTS

- A novel *n*-ZnSe/*p*-Sb_2Se_3/p^+-$AgInTe_2$ DH solar cell has been simulated using SCAPS-1D.
- $AgInTe_2$ BSF boosts PCE to 38.63% with V_{OC} = 0.86V and J_{SC} = 54.28 mA/cm^2, respectively.
- $AgInTe_2$ shows its potential as BSF in Sb_2Se_3-based DH solar cell in near future.

GRAPHICAL ABSTRACT

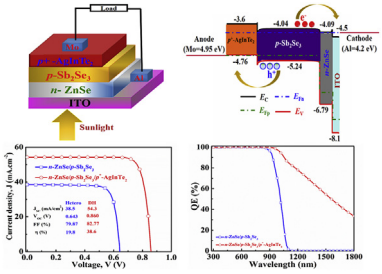

ARTICLE INFO

Keywords:
Sb_2Se_3
$AgInTe_2$
Dual-heterojunction
High efficiency
TSA upconversion

ABSTRACT

Here, we manifest the design and simulation of an *n*-ZnSe/*p*-Sb_2Se_3/p^+-$AgInTe_2$ dual-heterojunction (DH) solar cell which exhibits a prominent efficiency. The performance of the solar cell has been assessed with reported experimental parameters using SCAPS-1D simulator by varying thickness, doping concentration and defect density in each layer. The proposed structure shows an efficiency of 38.6% with V_{OC} = 0.860 V, J_{SC} = 54.3 mA/cm^2 and FF = 82.77%, respectively. Such a high efficiency close to Shockley-Queisser (SQ) limit of DH solar cell has been achieved as a result of the longer wavelength photon absorption in the p^+-$AgInTe_2$ back surface field (BSF) layer through a tail-states assisted (TSA) two-step photon upconversion phenomenon. These results indicate hopeful application of $AgInTe_2$ as a bottom layer in Sb_2Se_3-based solar cell to enhance the cell performance in future.

1. Introduction

In photovoltaic, a challenging part for researchers is obtaining a significant value of power conversion efficiency (PCE) along with selecting abundant low-cost and eco-friendly materials for large area production. The silicon solar cells are still dominating the present commercial markets although the highest PCE of the solar cells is just over 26% which has been reported in 2017 (Yoshikawa et al., 2017). Besides, Silicon's high melting point and minimal tolerance to defects in the manufacturing process necessitate a pricey processing environment (Steinmann et al., 2015). Additionally, higher production cost of wafer-based silicon solar cell and reduction of residential uses due to its fragility are the matter of concerns for traditional cells (Pathak et al., 2015; Bhopal et al., 2017). As a consequence, choice of alternative materials and simple fabrication process for evolution of cells have received enormous attention to the researchers (Tyagi et al., 2013).

Recently, different types of solar cells based on materials or fabrication process have received a great interest for capability of providing

* Corresponding author.
E-mail address: jak_apee@ru.ac.bd (J. Hossain).

https://doi.org/10.1016/j.heliyon.2022.e09120?tic>
Received 14 August 2021; Received in revised form 28 November 2021; Accepted 11 March 2022

significant efficiency. For instance, Cadmium telluride (CdTe) and CIGS based solar cells have clinched around 22% of PCE (Polman et al., 2016; Green et al., 2018; Jackson et al., 2016). Researchers have showed that recombination losses in the solar cells are resulted from the inherited dangling bonds at grain boundaries of Si as well as CdTe, CdS and CIGS that degrade the cell performance (Zhou et al., 2015). However, toxicity of materials in these types of solar cells are notable concerns for fabrication in industry due to health hazard (Pathak et al., 2015). Besides, scarcity of such elements causes rise in overall production cost. Therefore, replacement of cadmium containing materials has become a key concern (Pathak et al., 2014). Another option can be the hybrid methylammonium lead halide perovskite ($MAPbX_3$) based solar cell that has an efficiency of 20.1% but it exhibits insufficient tolerance to defects. More recently, the highest efficiency of 25.2% has been attained for perovskite solar cell by increasing charged carrier management (Yoo et al., 2021). Nevertheless, efficient perovskite solar cell uses harmful element lead (Pb) and exhibits lack of stability at low temperatures (Steinmann et al., 2015).

Antimony selenide, Sb_2Se_3 which has the simple single phase non-cubic orthorhombic chalcogenide structure can be a prominent absorber that can meet up all the constraints discussed above (Steinmann et al., 2015; Chen et al., 2017; Mavlonov et al., 2020; Guo et al., 2019; Shen et al., 2020). Such crystal structure tends to yield ribbon-like or layered morphologies that outcome with thoroughly anisotropic charge transport. However, Sb_2Se_3 is abundant on earth in the form of mineral subnite. Its thermal evaporation property at low temperature and vacuum (350 °C and ~8 mTorr, respectively) further contributes in cost minimization. It has also been found to exhibit excellent photovoltaic absorbance due to band gap of 1.1–1.3 eV and high absorption coefficient ($>10^5$ cm^{-1}) at visible portion of solar spectrum. Besides, Sb_2Se_3 displays a good carrier mobility ($\approx 15\ cm^2V^{-1}s^{-1}$). Literature reports indicate that both acceptor and donor types of impurities have been used for doping into the Sb_2Se_3 thin films that can be used as absorber layers in thin film solar cells. Many investigations have been performed on p and n type dopants of Sb_2Se_3 thin films. Among them, Cu, Sn and Fe can be employed as p-type dopants whereas halogen (I, Br, Cl) group can be utilized as n-type dopants in Sb_2Se_3 thin films (Mavlonov et al., 2020; Stoliaroff et al., 2020).

In 2009, researchers came up with 0.66% photo conversion efficiency introducing Sb_2Se_3 based solar cell structure (Messina et al., 2009). An efficiency of 6–7% for Sb_2Se_3-based solar cells have been obtained in experimental works through tuning selenization parameters and grain boundary inversion, respectively (Chen et al., 2018; Tang et al., 2019). Furthermore, contemporary work came into light with growth of nanorod array with a photo conversion efficiency of 9.2% (Li et al., 2019). However, simulation works have also been performed to provide guidelines for further improvement of Sb_2Se_3-based solar cells. According to recent simulation studies, the efficiency of the Sb_2Se_3-based solar cell can be reached to 23–29% by employing CdS window layer and CuO and $BaSi_2$ BSF layers (Li et al., 2019; Ahmed et al., 2021).

Zinc Selenide (ZnSe) can be an alternative solution to substitute toxic CdS in window layer for heterojunction solar cells. The efficiency of a photovoltaic cell relies on avoiding the recombination of photo generated carriers and such sidestepping is done by adding a thin window layer of a wide band gap material (Krause et al., 1994; Kale et al., 2006; Yater et al., 1996). ZnSe provides a wider band gap of 2.7eV than CdS of 2.4 eV (Ahmed et al., 2021). Another disadvantage is CdS window comes up with higher surface roughness and lower transmittance that limit the efficiency of the practical solar cells (Kim et al., 2010). To the contrary, polycrystalline nature and high refractive index of ZnSe provide higher transmittance in visible and ultraviolet region of solar spectrum (Jones and Woods, 1976; Green et al., 2010). Furthermore, low reaction to humidity of ZnSe is an additional advantage in industrial production (Yater et al., 1996).

Crossing the different cohort of solar modules, heterojunction solar cells has entered into fourth generation with a goal of overcoming the barriers of theoretical expectation (Sharma et al., 2015). A heterojunction is fabricated by attaching an n-type layer with a p-type layer of dissimilar materials. The absorption of photons in the absorber layer results photocurrent through the generation of electron-hole pairs which are separated by the space charges at the pn junction. However, the photo conversion efficiency of single heterojunction cells cannot go beyond the SQ limit due to (i) thermal relaxation loss by high energy photon absorbed by a low band gap substance and (ii) below-band gap absorption loss by excitation failure of low energy photon to a high band gap material (Malinkiewicz et al., 2014; Yamaguchi et al., 2018).

An improvement can be achieved with imparting comparatively higher band gap top layer and lower band gap back surface layer with absorbing material (Rong et al., 2018). Similar concepts have been found to overcome SQ limit for dual-heterojunction solar cells (Martí and Luque, 2015). $AgInTe_2$ is a potential ternary chalcopyrite material exhibiting a band gap of 0.96–1.16 eV which is just below the band gap of Sb_2Se_3 (Benseddik et al., 2020; El-Korashy et al., 1999). Such a value along with high absorption coefficient (4×10^4 cm^{-1} at an wavelength of 1095 nm) and also sub-band gap effects have brought it as a suitable candidate for back surface absorber layer (El-Korashy et al., 1999). Though several works have been found on $AgInTe_2$ based solar cells, to the best of our knowledge, such a promising candidate has never been utilized as a BSF layer.

In this work, a novel Sb_2Se_3-based *n*-ZnSe/*p*-Sb_2Se_3/p^+-$AgInTe_2$ dual-heterojunction solar cell structure has been proposed and simulated with a view to provide longer wavelength light absorption and minimize

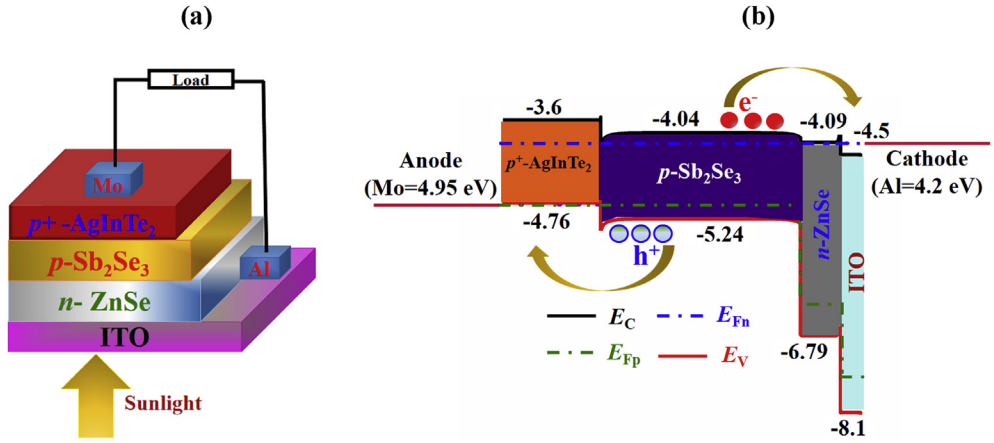

Figure 1. The (a) schematic block diagram and (b) energy band diagram with illumination of *n*-ZnSe/*p*-Sb_2Se_3/p^+-$AgInTe_2$ dual-heterojunction solar cell.

photon loss in the back surface layer. The light trapping strategy and the reason of high efficiency have been illustrated with absorption of photon in Sb_2Se_3 absorber layer through tail-states assisted (TSA) two-step photon upconversion phenomenon in p^+-$AgInTe_2$ BSF as well as bottom absorber layer.

2. Design of proposed Sb_2Se_3-based dual-heterojunction and numerical simulation

2.1. Device structure

The schematic block diagram and illuminated energy band diagram of the proposed highly efficient Sb_2Se_3-based dual-heterojunction solar cell are visualized in Figure 1a and b, respectively. Herein, photons enter through the Indium tin oxide (ITO) coated glass substrate and n-type ZnSe window layer. The photons are then absorbed by p-type Sb_2Se_3 absorber layer. The E_C and E_V of ZnSe are 4.09 and 6.79 eV, respectively (Olopade et al., 2012; Samantilleke et al., 1998). On the other hand, the electron affinity and ionization potential of Sb_2Se_3 are 4.04 and 5.24 eV, respectively. Hence, it creates a possibility for n-type ZnSe and p-type Sb_2Se_3 to build a favorable pn junction. In addition, $AgInTe_2$ is a semiconducting compound having a direct band gap of 0.96–1.16 eV which has already been reported as absorber layer with CdTe window combination (Benseddik et al., 2020). In this design, p^+-type $AgInTe_2$ has been employed to perform double role such as bottom absorber and back surface field (BSF) layer. Because of its high absorption coefficient (α) i.e sub-band gap absorption in the longer wavelength region, it is an efficient material as bottom absorber layer to absorb longer wavelength photons (El-Korashy et al., 1999; Vaidhyanathan et al., 1983). $AgInTe_2$ has electron affinity and ionization potential of 3.6 eV and 4.76 eV, respectively making it a suitable candidate to form a pp^+ junction with Sb_2Se_3. The quasi Fermi levels for electrons and holes are denoted as E_{Fn} and E_{Fp}, respectively as depicted in Figure 1b. In $AgInTe_2$, the E_{Fn} level lies above the VB edge whereas E_{Fp} level lies below the CB edge in ZnSe. Therefore, photo-generated electrons are moved towards the *n*-type window layer and blocked by BSF layer. Consequently, photo-generated holes are blocked by window layer and moved towards p^+-type BSF layer. Therefore, anode and cathode can easily collect holes and electrons, respectively from absorber layer. In this design, earth abundant metals Al and Mo are used as cathode and anode, respectively.

2.2. Simulation model and physical parameters

The Sb_2Se_3-based *n*-ZnSe/*p*-Sb_2Se_3/p^+-$AgInTe_2$ dual-heterojunctionsolar cell was numerically simulated using a one-dimensional solar cell capacitance (SCAPS-1D) software developed by M. Burgelman et al. at the University of Gent, Belgium (Burgelman et al., 2004). This software analyzes solar cell structure by solving three basic equations of semiconductor i.e. Poisson's equation, the continuity equations for free holes and electrons and the drift-diffusion equation. The simulation was accomplished under the illumination of one sun with 100 mW/cm^2 and the global air mass (AM) of 1.5G illumination spectrum at 300 K operating temperature. In this simulation, ideal values of series and shunt resistance were considered and radiative recombination coefficient was avoided. Gaussian energetic distribution was set for acceptor and donor defects for bulk layers and interface defects were also considered. Thermal velocity of 10^7 cm/s was set for window, absorber and BSF layer and surface recombination velocity was taken 10^7 cm/s for both metallic contacts. The absorption coefficient data for ZnSe, Sb_2Se_3 and $AgInTe_2$ layer were collected from various literatures based on experimental works (El-Korashy et al., 1999; Adachi and Taguchi, 1991; El-Shair et al., 1991). It is noted that SCAPS software can automatically account the sub-band gap absorption effect on solar cell performance once the optical data are provided. The physical parameters for different layers used in this simulation are shown in Table 1, whereas interfaces parameters are shown in Table 2.

Table 1. Physical parameters of *n*-ZnSe/*p*-Sb_2Se_3/p^+-$AgInTe_2$ dual-heterojunction solar cell used in this simulation.

Parameters	ITO (Ahmmed et al., 2020)	*n*-ZnSe (Olopade et al., 2012; Samantilleke et al., 1998)	*p*-Sb_2Se_3 (Z. Q. Li et al., 2019)	p^+-$AgInTe_2$ (Benseddik et al., 2020; El-Korashy et al., 1999; Yang et al., 2017)
Layer type	Substrate	Window	Absorber	BSF
[a]Thickness [μm]	0.05	0.1	1.0	0.5
Band gap, E_g [eV]	3.6	2.7	1.2	1.16
Electron affinity, χ [eV]	4.5	4.09	4.04	3.6
Dielectric permittivity, ε [relative]	8.9	10	18	8.9
Effective CB density, N_C [cm^{-3}]	2.2×10^{18}	1.5×10^{18}	2.2×10^{18}	3.66×10^{19}
Effective VB density, N_V [cm^{-3}]	1.8×10^{19}	1.8×10^{19}	1.8×10^{19}	1.35×10^{19}
Electron mobility, μ_n [$cm^2\ V^{-1}\ s^{-1}$]	50	50	15	1011
Hole mobility, μ_p [$cm^2\ V^{-1}\ s^{-1}$]	10	20	5.1	887
[a]Donor concentration, N_D [cm^{-3}]	1.0×10^{21}	1.0×10^{18}	0	0
[a]Acceptor concentration, N_A [cm^{-3}]	1.0×10^{7}	0	1.0×10^{15}	3.5×10^{19}
Defect type	Acceptor	Acceptor	Donor	Neutral/Donor
Energetic distribution	Gaussian	Gaussian	Gaussian	Gaussian
Reference for defect energy level, E_t	Above the highest E_V	Above the highest E_V	Above the highest E_V	Above the highest E_V
Energy with respect to Reference [eV]	1.8	1.35	0.6	0.58
[a]Peak defect density, $N(t)$ [$eV^{-1}\ cm^{-3}$]	1.0×10^{14}	1.0×10^{13}	1.0×10^{13}	1.0×10^{13}
Characteristic energy [eV]	0.1	0.1	0.1	0.1
Electron capture cross section for defect [cm^2]	10^{-15}	10^{-15}	10^{-15}	10^{-15}
Hole capture cross section for defect [cm^2]	10^{-15}	10^{-15}	10^{-17}	10^{-15}

[a)] is a variable field.

Table 2. Interface parameters used in this simulation.

Parameters	ZnSe/Sb_2Se_3 interface	Sb_2Se_3/$AgInTe_2$ interface
Defect type	Neutral	Neutral
Capture cross section for electrons [cm^2]	10^{-19}	10^{-19}
Capture cross section for holes [cm^2]	10^{-19}	10^{-19}
Energetic distribution	Single	Single
Reference for defect energy level, E_t	Above the highest E_V	Above the highest E_V
Energy with respect to reference (eV)	0.6	0.6
Total defects (cm^{-2})	10^{10}	10^{10}

3. Results and discussion

3.1. Performance of Sb_2Se_3-based solar cells

3.1.1. Role of Sb_2Se_3 absorber layer on PV parameters of n-ZnSe/p-Sb_2Se_3 solar cell

In this section, the impacts of thickness, carrier concentration and bulk defects of absorber layer on the proposed Sb_2Se_3-based solar cell without BSF layer have been studied. Figure 2a depicts the dependency of solar cell performance on thickness of Sb_2Se_3 absorber layer considering 10^{15} and 10^{13} cm^{-3} as acceptor concentration and defect density, respectively. Here, we observe that as the thickness of Sb_2Se_3 absorber layer is increased, all photovoltaic (PV) parameters boost as well. The short circuit, J_{SC} has been risen up from 36.4 to 40.1 mA/cm^2 with an increase in thickness from 0.5 to 3.0 μm. The increment of J_{SC} is reasonable because thicker absorber layer can create more electron-hole pairs (EHPs) through absorbing more photons incident on it (Hossain et al., 2020). At the same time, open circuit voltage, V_{OC} also increases with the thickness of the Sb_2Se_3 absorber layer. For instance, V_{OC} goes from 0.587 to 0.693 V at an enlargement of absorber thickness from 0.5 to 3.0 μm. The obtained V_{OC} of 0.680 V at 2.0 μm thickness of Sb_2Se_3 is consistent with the previous report (Kale et al., 2006). The fill factor (*FF*) and PCE have also ameliorated from 80.38 and 17.2 % to 82.82% and 22.9%, respectively at an increment of Sb_2Se_3 absorber from 0.5 to 3.0 μm. We consider 1.0 μm as the optimized thickness of the absorber Sb_2Se_3 layer to carry out further investigations.

The effect of acceptor concentration of Sb_2Se_3 absorber layer on PV parameters are shown in Figure 2b. The V_{OC} rises from 0.601 to 0.788 V when the carrier concentration is increased from 10^{13} to 10^{17} cm^{-3}. However, J_{SC} is observed to downfall with the increase in carrier concentration. The recombination loss increases as a result of high doping concentration that affect the cell performance and a decrement of J_{SC} occurres from 38.5 to 35.9 mA/cm^2 due to the enhancement of carrier concentration from 10^{13} to 10^{17} cm^{-3} (Hossain et al., 2020; Watahiki

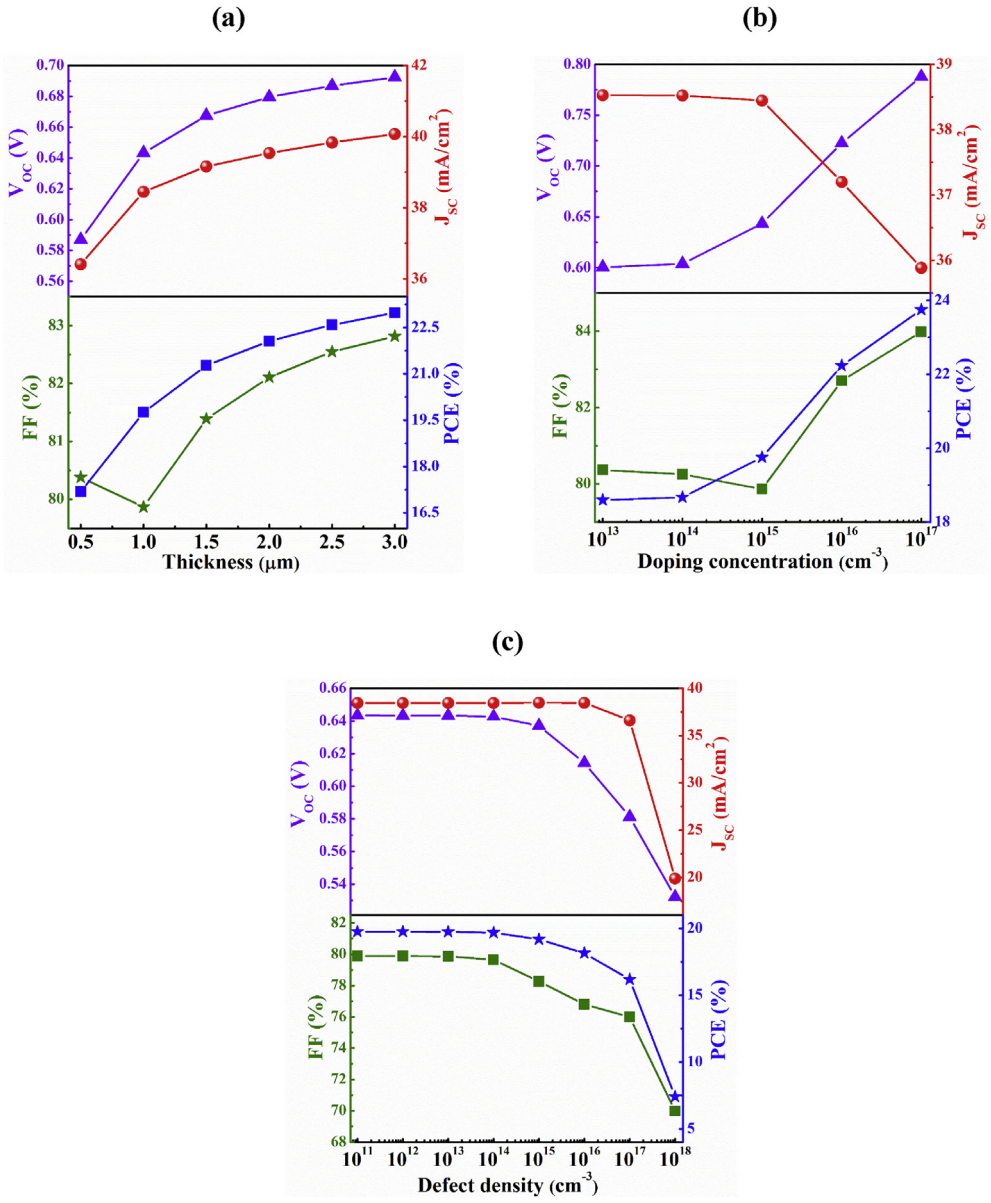

Figure 2. Performance dependency of n-ZnSe/p-Sb_2Se_3 solar cell on Sb_2Se_3 absorber layer parameters: (a) thickness, (b) doping concentration and (c) bulk defects.

et al., 2016). However, as the series resistance gets lowered at higher carrier concentration, FF rises from 80.37 to 84%. Consequently, the PCE enhances from 18.60 to 23.75% depending on upgradation of V_{OC} and *FF*.

Defects play an important role in the performances of a solar cell. A number of investigations have been done on defects formation in Sb_2Se_3 for determining formation energy and transition levels that might be helpful for the improvement of the performance of Sb_2Se_3 based solar cells (Mavlonov et al., 2020; Savory and Scanlon, 2019; Stoliaroff et al., 2020). The variation of PV parameters with bulk defects of Sb_2Se_3 absorber layer is delineated in Figure 2c. To study the dependency of output parameters on defects of Sb_2Se_3 absorber layer, single donor type defects in the range from 10^{11} to 10^{18} cm^{-3} have been assumed. It is observed from the figure that the J_{SC} is about 38.45 mA/cm^2 and is almost independent on bulk defects of absorber up to a defect of 10^{16} cm^{-3}. However, if the bulk defect is further increased to 10^{17} cm^{-3}, J_{SC} decreases to 36.6 mA/cm^2 and the reduction of the photocurrent is about 1.8 mA/cm^2. The photocurrent drastically plunges to 19.9 mA/cm^2 at a defect of 10^{18} cm^{-3} owing to the increase in recombination current with defects (Kuddus et al., 2021b). The other parameters are also affected by the bulk defects. The Shockley-Read-Hall (SRH) recombination becomes the dominant recombination at high defects resulting inflation in the reverse saturation current and consequently V_{OC} of the device reduces (Moon et al., 2020). Here, The V_{OC} drops from 0.644 to 0.532 V when the defect density is raised from 10^{11} to 10^{18} cm^{-3}. The *FF* also drops from 79.89 to 69.98% due to defects of absorber layer. As all the parameters gets reduced due to the increment of bulk defects of Sb_2Se_3 layer, the PCE of the solar cell also drastically turns down from 19.8% at defects of 10^{11} cm^{-3} to 7.4% at defects of 10^{18} cm^{-3}. We have considered 10^{13} cm^{-3} as reasonable optimized defects for Sb_2Se_3 absorber layer.

The maximum efficiency of Sb_2Se_3-based solar cell without BSF layer is found to be about 23.8% with a high acceptor concentration of 10^{17} cm^{-3} and a thickness of 1.0 μm. Moreover, it has been observed that ZnSe window layer has negligible effects on the output parameters. Therefore, the optimized PCE of the Sb_2Se_3 solar cell without BSF layer is 19.8% with acceptor concentration and thickness of 10^{15} cm^{-3} and 1.0 μm, respectively.

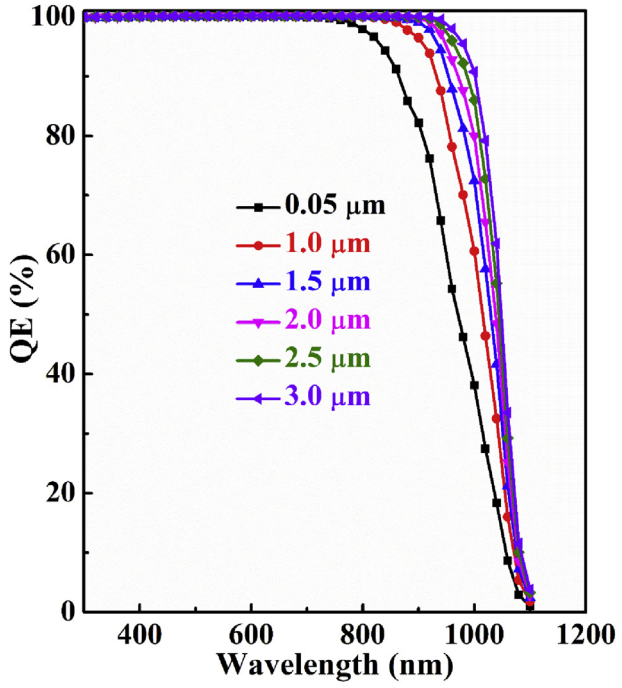

Figure 3. Simulated QE dependence on Sb_2Se_3 absorber layer thickness of n-ZnSe/p-Sb_2Se_3 single-heterojunction solar cell.

3.1.2. Role of Sb_2Se_3 absorber layer on quantum efficiency of n-ZnSe/p-Sb_2Se_3 solar cell

The quantum efficiency (QE) is a function of light wavelength (λ) which can be defined as the ratio of charge carriers produced by a solar cell to the number of incident photons on that cell (Hossain et al., 2021b; Moon et al., 2020). Figure 3 represents the simulated QE with respect to thickness of Sb_2Se_3 absorber layer of *n*-ZnSe/*p*-Sb_2Se_3 single heterojunction solar cell. It is noticed in the figure that QE improves gradually with the extension of Sb_2Se_3 absorber layer thickness as thicker absorber layer can capture more photons. Then all the curves associated different thickness downfall towards 0% at a particular higher wavelength when photon energy (hν) becomes lower than band gap (E_g) energy of Sb_2Se_3 absorber layer.

3.2. Sb_2Se_3-based solar cell with $AgInTe_2$ BSF layer

3.2.1. Role of $AgInTe_2$ layer on PV parameters of n-ZnSe/p-Sb_2Se_3/p^+-$AgInTe_2$ dual-heterojunction solar cell

In this section, the influences of $AgInTe_2$ layer on the designed *n*-ZnSe/*p*-Sb_2Se_3/p^+-$AgInTe_2$ dual-heterojunction structure have been explored. The thickness, doping concentration, and bulk defects of the $AgInTe_2$ BSF layer have been varied in order to investigate the impact of this BSF layer as displayed in Figure 4.

Figure 4a exhibits the thickness dependent PV parameters of *n*-ZnSe/*p*-Sb_2Se_3/p^+-$AgInTe_2$ dual-heterojunction solar cell. As observed, all of the output parameters significantly improve on account of employing $AgInTe_2$ layer that performs dual role as BSF and bottom absorber layer. Here, J_{SC} escalates from 38.5 to 54.3 mA/cm^2 with an addition of 0.5 μm thick $AgInTe_2$ layer. When the thickness of $AgInTe_2$ is extended from 0.1 to 0.9 μm, J_{SC} enhances from 43.6 to 58.7 mA/cm^2. The significant growth of J_{SC} relies on the absorption of longer wavelength photons by $AgInTe_2$ layer through Tail-States-Assisted (TSA) two-steps photon upconversion process (Mostaque et al., 2022; Mondal et al., 2021; Kuddus et al., 2021a). In TSA upconversion process, two low-energy i.e. sub-band gap photons are absorbed in a sequence by Urbach tail-states of materials which provide extra EHPs. A material with preferable band gap, doping concentration and high absorption coefficient in longer wavelength region could result TSA upconversion process (Mostaque et al., 2022; Mondal et al., 2021; Hossain et al., 2021a, 2022). The detail qualitative discussion of the TSA upconversion process can be perceived in other work (Mostaque et al., 2022). Fortunately, $AgInTe_2$ is a chalcopyrite material comprising a band gap of 1.16 eV (Malinkiewicz et al., 2014), high absorption coefficient of 10^3 cm^{-1} in the wavelength of 1800 nm (obtained from SCAPS extrapolation utilizing absorption coefficient data from experimental work) (Benseddik et al., 2020; El-Korashy et al., 1999) and also possesses high carrier concentration of 3.66×10^{19} cm^3 (Yang et al., 2017). All of these factors make $AgInTe_2$ a suitable candidate to participate in a TSA upconversion process. The V_{OC} also improves from 0.640 to 0.840 V due to insertion of 0.5 μm $AgInTe_2$ layer. The V_{OC} gradually enhances from 0.851 at 0.1 μm to 0.863 V at 0.9 μm thickness of $AgInTe_2$. The insertion of $AgInTe_2$ layer produces high built-in potential in the Sb_2Se_3/$AgInTe_2$ interface which contribute to the enhancement of the V_{OC} (Hossain et al., 2021b; Mondal et al., 2021). The FF appears to be almost constant as a function of the thickness of $AgInTe_2$. As J_{SC} and V_{OC} both rises with varying depth from 0.1 to 0.9 μm, a negligible change from 82.94 to 82.73% has been observed in FF. Eventually, the insertion of $AgInTe_2$ BSF layer enriches the PCE from 30.8 to 41.9% as the width of BSF layer is expanded from 0.1 to 0.9 μm owing to the excessive gain in current and voltage. An enhancement of PCE from 19.8 to 38.6% has been observed at 0.5 μm thickness of $AgInTe_2$ BSF layer.

Figure 4b delineates the performances of the proposed Sb_2Se_3-based DH solar cell structure with the variation of acceptor concentration (N_A) of $AgInTe_2$ layer from 10^{16} to 10^{21} cm^{-3} while maintaining the other

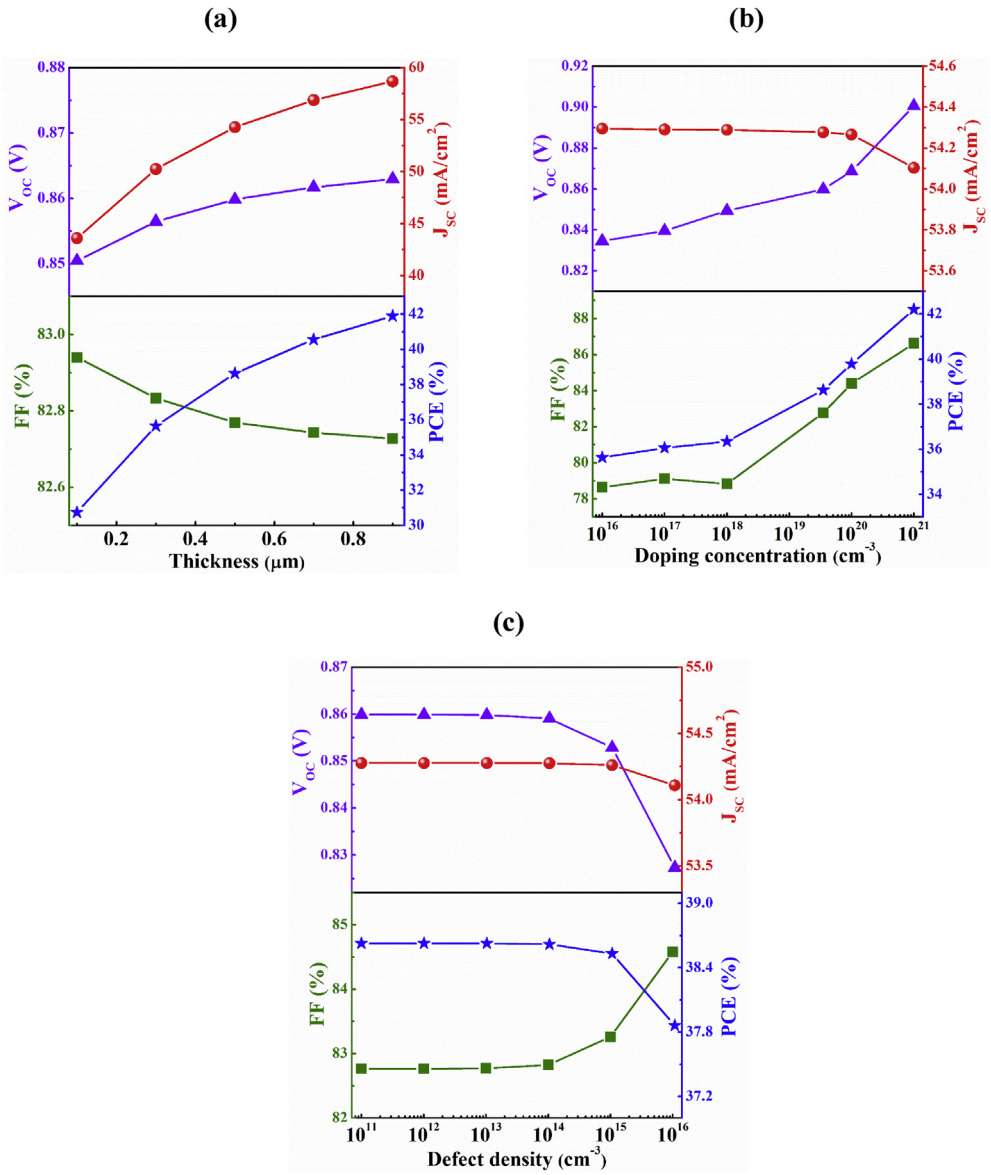

Figure 4. Dependency of the performance of *n*-ZnSe/*p*-Sb_2Se_3/p^+-$AgInTe_2$ dual-heterojunction solar cell on $AgInTe_2$ BSF layer parameters: (a) thickness, (b) doping concentration and (c) bulk defects.

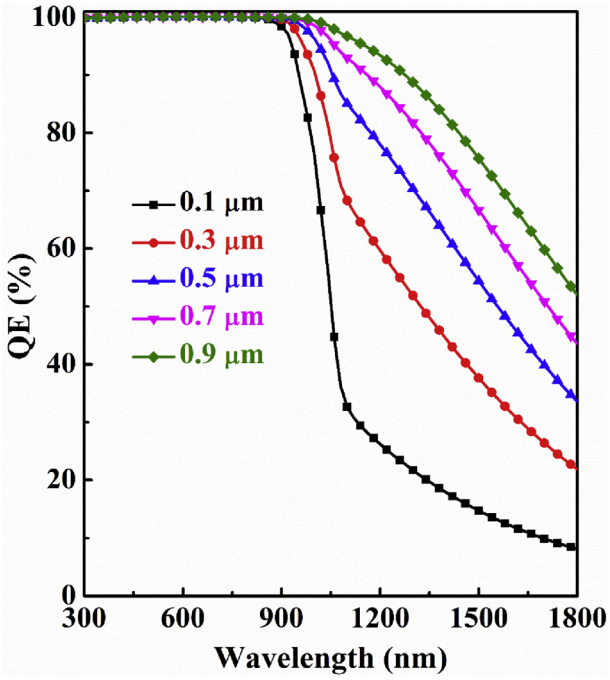

Figure 5. Simulated QE dependence of n-ZnSe/p-Sb_2Se_3/p^+-$AgInTe_2$ dual-heterojunction solar cell on the thickness of $AgInTe_2$layer.

parameters unchanged. It is observed from figure that the J_{SC} is almost constant up to the concentration of 10^{20} cm^{-3}. It slightly falls from 54.3 to 54.1 mA/cm^2 due to high carrier concentration which may happened due to the parasitic free carrier absorption or high doping may have negative effect in TSA upconversion process in the BSF layer (Kuddus et al., 2021a). The V_{OC} escalates from 0.835 to 0.901 V with increasing acceptor concentration from 10^{16} to 10^{21} $cm^{-3}$of $AgInTe_2$ layer. Since the built-in potential rises with additional N_A, the enhancement of V_{OC} with doping concentration is reasonable since higher built-in potential will the reduce recombination current (Hossain et al., 2020; Mostaque et al., 2022). This trend is also evident in *FF* and PCE which elevate from 78.65 and 35.7% to 86.62 and 42.2%, respectively for the increase of carrier concentration from 10^{16} to 10^{21} cm^{-3}.

To investigate the influences of defect density of $AgInTe_2$ BSF layer, on Sb_2Se_3-based double-heterojunction solar cell, neutral/donor types of defects have been assumed and varied it from 10^{11} to 10^{16} cm^{-3} considering other parameters same as specified in Tables 1 and 2. The variation of photovoltaic parameters with bulk defects of $AgInTe_2$ layer is depicted in Figure 4c. The J_{SC} shows almost constant behavior up to a defect level of 10^{15} cm^{-3} but then it has negligible decrement because of higher defects which obstruct to generate EHPs. The V_{OC} also drops from 0.860 to 0.827 V owing to the increase of defect level from 10^{11} to 10^{16} cm^{-3}. Since, both J_{SC} and V_{OC} fall with increasing bulk defects of $AgInTe_2$ layer, *FF* is found to improve from 82.76 to 84.58%. The PCE has also decreased from 38.6% at defect density of 10^{11} cm^{-3} to 37.9% at defect density of 10^{16} cm^{-3}. Hence, utilizing $AgInTe_2$ as BSF as well as bottom absorber layer in Sb_2Se_3 solar cell with reasonable defects, it is possible to attain the Shockley-Queisser (SQ) efficiency limit for a dual-heterojunction solar cell.

3.2.2. Role of $AgInTe_2$ layer on quantum efficiency of n-ZnSe/p-Sb_2Se_3/p^+-$AgInTe_2$ dual-heterojunction solar cell

Figure 5 represents the simulated QE as a function of light wavelength for Sb_2Se_3-based dual-heterojunction solar cell with a varying thickness of $AgInTe_2$ layer. It is noticed that, QE increases dramatically as the thickness of the $AgInTe_2$ layer is gradually incremented from 0.1μm to 0.9 μm. In the longer wavelength range, for example, at 1800 nm, this device has a QE of over 30% at 0.5 m thickness, whereas 0% QE in absence of the $AgInTe_2$ layer as observed in Figure 3. It clarifies the ability of $AgInTe_2$ layer to capture longer wavelength photons as demonstrated by the TSA two-steps photon upconversion process in which the creation of additional EHPs plays a significant role behind this augmentation (Mostaque et al., 2022; Mondal et al., 2021; Kuddus et al., 2021a).

3.3. The optimized performance of single and dual-heterojunction cells

The current-voltage curves under illumination and quantum efficiency for Sb_2Se_3-based single *n-p* heterojunction and double *n-p-*p^+ heterojunction solar cells are displayed in Fig. 6a and b, respectively. It is evident from Figure 6a that the installation of a p + -$AgInTe_2$ layer revamps the cell performance substantially. The reason behind such an overshoot can be demonstrated with the TSA photon upconversion process where sub-band gap photons are occupied by the Urbach states (Mostaque et al., 2022; Mondal et al., 2021; Kuddus et al., 2021a). These low energy sub-band gap photons take part in generating electron-hole pairs contributing to the photocurrent (Yablonovitch et al., 1982; Wu and Williams, 1983). The degree of current enhancement and hence QE depend not only on Urbach energy but also on the band gap of the material. The generation of high built-in potential at the Sb_2Se_3/$AgInTe_2$ interface further enhances the value of V_{OC} (Hossain et al., 2021b). As a result, the efficiency has remarkably improved due to the addition of $AgInTe_2$ as bottom layer. Figure 6b reveals that the QE in *n-p* heterojunction structure falls to 0% at the wavelength of 1100 nm whereas, it displays about 40% corresponding QE in the proposed *n-p-*p^+ structure with the inclusion of $AgInTe_2$ BSF layer. The QE seems to theoretically

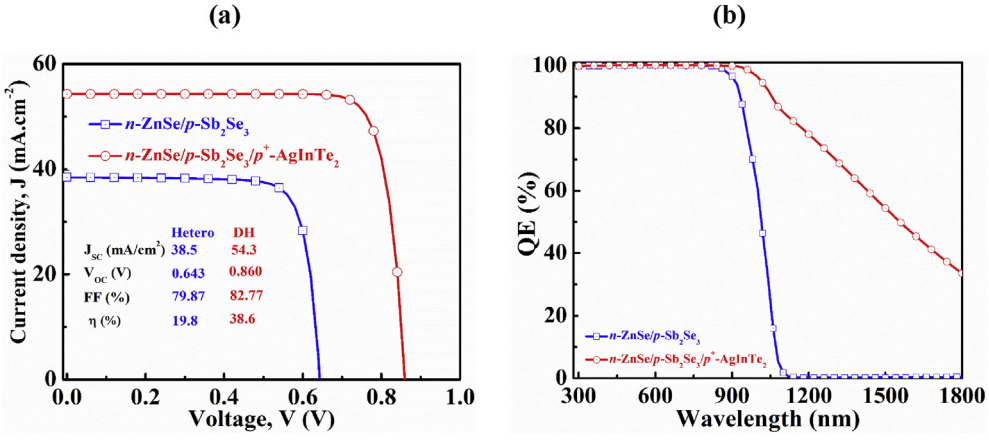

Figure 6. Simulated (a) light J-V and (b) QE curves of Sb_2Se_3-based single and dual-heterojunction solar cells.

remain around 30% even for 1800 nm wavelength. This finding indicates that $AgInTe_2$ could be a promising candidate for improving the PCE of Sb_2Se_3-based solar cells in near future.

4. Conclusion

The present work demonstrates the numerical simulation of Sb_2Se_3-based *n*-ZnSe/*p*-Sb_2Se_3/p^+-$AgInTe_2$ dual-heterojunction solar cell using SCAPS-1D software by incorporating interface defects and varying thickness, doping concentration and bulk defects in each layer. The simulation reveals that the incorporation of $AgInTe_2$ which also serves as a bottom absorber layer can collect longer wavelength photons through TSA two-steps photon upconversion process, resulting a considerable enhancement in photocurrent. The optimized performance considering 0.1 μm thick *n*-ZnSe window and 1.0 μm *p*-Sb_2Se_3 absorber provides an efficiency of 19.8% that shoots up to 38.6% with J_{SC} of 54.3 mA/cm^2, V_{OC} of 0.860 V and *FF* of 82.77%, respectively owing to the incorporation of only a 0.5 μm $AgInTe_2$ BSF layer. Overall, the study suggests that $AgInTe_2$ compound as a bottom layer displays strong potential for the enhancement of the efficiency of Sb_2Se_3-based solar cells in future.

Declarations

Author contribution statement

Bipanko Kumar Mondal: Conceived and designed the experiments; Performed the experiments; Analyzed and interpreted the data; Wrote the paper.

Shaikh Khaled Mostaque: Analyzed and interpreted the data; Wrote the paper.

Jaker Hossain: Conceived and designed the experiments; Contributed reagents, materials, analysis tools or data; Wrote the paper.

Funding statement

This research did not receive any specific grant from funding agencies in the public, commercial, or not-for-profit sectors.

Data availability statement

Data included in article/supplementary material/referenced in article.

Declaration of interests statement

The authors declare no conflict of interest.

Additional information

No additional information is available for this paper.

Acknowledgements

The authors highly appreciate Dr. Marc Burgelman, University of Gent, Belgium, for providing SCAPS 1D simulation software.

References

Adachi, S., Taguchi, T., 1991. Optical properties of ZnSe. Phys. Rev. B 43, 9569–9577.

Ahmed, S.R. Al, Sunny, A., Rahman, S., 2021. Performance enhancement of Sb_2Se_3 solar cell using a back surface field layer: a numerical simulation approach. Sol. Energy Mater. Sol. Cells 221, 110919.

Ahmmed, S., Aktar, A., Hossain, J., Ismail, A.B.M., 2020. Enhancing the open circuit voltage of the SnS based heterojunction solar cell using NiO HTL. Sol. Energy 207, 693–702.

Benseddik, N., Belkacemi, B., Boukabrine, F., Ameur, K., Mazari, H., Boumesjed, A., Benyahya, N., Benamara, Z., 2020. Numerical study of $AgInTe_2$ solar cells using SCAPS. Adv. Mater. Process. Technol.

Bhopal, M.F., Lee, D.W., Rehman, A.U., Lee, S.H., 2017. Past and future of graphene/silicon heterojunction solar cells: a review. J. Mater. Chem. C 5, 10701–10714.

Burgelman, M., Verschraegen, Degrave, J.S., Nollet, P., 2004. Modeling thin-film devices. Prog. Photovoltaics Res. Appl. 12, 143–153.

Chen, C., Bobela, D.C., Yang, Y., Lu, S., Zeng, K., Ge, C., Yang, B., Gao, L., Zhao, Y., Beard, M.C., Tang, J., 2017. Characterization of basic physical properties of Sb_2Se_3 and its relevance for photovoltaics. Front. Optoelectron. 10, 18–30.

Chen, C., Li, K., Chen, S., Wang, L., Lu, S., Liu, Y., Li, D., Song, H., Tang, J., 2018. Efficiency improvement of Sb_2Se_3solar cells via grain boundary inversion. ACS Energy Lett 3, 2335–2341.

El-Korashy, A., Abdel-Rahim, M.A., El-Zahed, H., 1999. Optical absorption studies on $AgInSe_2$ and $AgInTe_2$ thin films. Thin Solid Films 338, 207–212.

El-Shair, H., Ibrahim, A., Abd El-Wahabb, E., Afify, M., Abd El-Salam, F., 1991. Optical properties of Sb_2Se_3 thin films. Vacuum 42, 911–914.

Green, M.A., Emery, K., Hishikawa, Y., Warta, W., 2010. Solar cell efficiency tables (version 36). Prog. Photovoltaics Res. Appl. 18, 346–352.

Green, M.A., Hishikawa, Y., Dunlop, E.D., Levi, D.H., Hohl-Ebinger, J., Ho-Baillie, A.W.Y., 2018. Solar cell efficiency tables (version 51). Prog. Photovoltaics Res. Appl. 26, 3–12.

Guo, L., Grice, C., Zhang, B., Xing, S., Li, L., Qian, X., Yan, F., 2019. Improved stability and efficiency of CdSe/Sb_2Se_3 thin-film solar cells. Sol. Energy 188, 586–592.

Hossain, J., Rahman, M., Moon, M.M.A., Mondal, B.K., Rahman, M.F., Rubel, M., 2020. Guidelines for a highly efficient CuI/n-Si heterojunction solar cell. Eng. Res. Exp. 2, 045019.

Hossain, J., Mondal, B.K., Mostaque, S.K., 2022. Computational investigation on the photovoltaic performance of an efficient GeSe-based dual-heterojunction thin film solar cell. Semicond. Sci. Technol. 37, 015008 (Accepted).

Hossain, J., Mondal, B.K., Mostaque, S.K., 2021a. Design of a highly efficient FeS_2-based dual-heterojunction thin film solar cell. Int. J. Green Energy (Accepted).

Hossain, J., Mahabub Alam Moon, M., Mondal, B.K., Halim, M.A., 2021b. Design guidelines for a highly efficient high-purity germanium (HPGe)-based double-heterojunction solar cell. Opt Laser. Technol. 143, 107306.

Jackson, P., Wuerz, R., Hariskos, D., Lotter, E., Witte, W., Powalla, M., 2016. Effects of heavy alkali elements in Cu(In,Ga)Se_2 solar cells with efficiencies up to 22.6. Phys. Status Solidi Rapid Res. Lett. 10, 583–586.

Jones, G., Woods, J., 1976. The electrical properties of zinc selenide. J. Phys. D Appl. Phys. 9, 799.

Kale, R.B., Sartale, S.D., Ganesan, V., Lokhande, C.D., Lin, Y.F., Lu, S.Y., 2006. Room temperature chemical synthesis of lead selenide thin films with preferred orientation. Appl. Surf. Sci. 253, 930–936.

Kim, M.J., Kim, H.T., Kang, J.K., Kim, D.H., Lee, D.H., Lee, S.H., Sohn, S.H., 2010. Effects of the surface roughness on optical properties of CdS thin films. Mol. Cryst. Liq. Cryst. 532, 21/[437]-28/[444].

Krause, E., Hartmann, H., Menninger, J., Hoffmann, A., Fricke, C., Heitz, R., Lummer, B., Kutzer, V., Broser, I., 1994. Influence of growth non-stoichiometry on optical properties of doped and non-doped ZnSe grown by chemical vapour deposition. J. Cryst. Growth 138, 75–80.

Kuddus, A., Ismail, A.B.M., Hossain, J., 2021a. Design of a highly efficient CdTe-based dual heterojunction solar cell with 44% predicted efficiency. Sol. Energy 221, 488–501.

Kuddus, A., Mostaque, S.K., Hossain, J., 2021b. Simulating the performance of a high-efficiency SnS-based dual-heterojunction thin film solar cell. Opt. Mater. Express 11, 3812–3826.

Li, Z., Liang, X., Li, G., Liu, H., Zhang, H., Guo, J., Chen, J., Shen, K., San, X., Yu, W., Schropp, R.E.I., Mai, Y., 2019a. 9.2%-efficient core-shell structured antimony selenide nanorod array solar cells. Nat. Commun. 10, 125.

Li, Z.Q., Ni, M., Feng, X.D., 2019b. Simulation of the Sb_2Se_3 solar cell with a hole transport layer. Mater. Res. Express 7, 016416.

Malinkiewicz, O., Yella, A., Lee, Y.H., Espallargas, G.M., Graetzel, M., Nazeeruddin, M.K., Bolink, H.J., 2014. Perovskite solar cells employing organic charge-transport layers. Nat. Photonics 8, 128–132.

Martí, A., Luque, A., 2015. Three-terminal heterojunction bipolar transistor solar cell for high-efficiency photovoltaic conversion. Nat. Commun. 6, 6902.

Mavlonov, A., Razykov, T., Raziq, F., Gan, J., Chantana, J., Kawano, Y., Nishimura, T., Wei, H., Zakutayev, A., Minemoto, T., Zu, X., Li, S., Qiao, L., 2020. A review of Sb_2Se_3 photovoltaic absorber materials and thin-film solar cells. Sol. Energy 201, 227–246.

Messina, S., Nair, M.T.S., Nair, P.K., 2009. Antimony selenide absorber thin films in all-chemically deposited solar cells. J. Electrochem. Soc. 156, H327.

Mondal, B.K., Mostaque, S.K., Rashid, M.A., Kuddus, A., Shirai, H., Hossain, J., 2021. Effect of CdS and In_3Se_4 BSF layers on the photovoltaic performance of PEDOT:PSS/n-Si solar cells: simulation based on experimental data. Superlattice. Microst. 152, 106853.

Moon, M.M.A., Ali, M.H., Rahman, M.F., Hossain, J., Ismail, A.B.M., 2020. Design and simulation of $FeSi_2$-based novel heterojunction solar cells for harnessing visible and near-infrared light. Phys. Status Solid. Appl. Mater. Sci. 217, 1900921.

Mostaque, S.K., Mondal, B.K., Hossain, J., 2022. Simulation approach to reach the SQ limit in CIGS-based dual-heterojunction solar cell. Optik 249, 168278.

Olopade, M.A., Oyebola, O.O., Adeleke, B.S., 2012. Investigation of some materials as buffer layer in copper zinc tin sulphide (Cu_2ZnSnS_4) solar cells by SCAPS-1D. Pelagia Res. Libr. Adv. Appl. Sci. Res. 3, 3396–3400.

Pathak, D., Wagner, T., Adhikari, T., Nunzi, J.M., 2015. Photovoltaic performance of $AgInSe_2$-conjugated polymer hybrid system bulk heterojunction solar cells. Synth. Met. 199, 87–92.

Pathak, D., Wagner, T., Šubrt, J., Kupcik, J., 2014. Characterization of mechanically synthesized $AgInSe_2$ nanostructures. Can. J. Phys. 92, 1–8.

Polman, A., Knight, M., Garnett, E.C., Ehrler, B., Sinke, W.C., 2016. Photovoltaic materials: present efficiencies and future challenges. Science 352, aad4424 aad4424.
Rong, Y., Hu, Y., Mei, A., Tan, H., Saidaminov, M.I., Seok, S. Il, McGehee, M.D., Sargent, E.H., Han, H., 2018. Challenges for commercializing perovskite solar cells. Science 361, 1214.
Samantilleke, A.P., Boyle, M.H., Young, J., Dharmadasa, I.M., 1998. Growth of n-type and p-type ZnSe thin films using an electrochemical technique for applications in large area optoelectronic devices. J. Mater. Sci. Mater. Electron. 9, 231–235.
Savory, C.N., Scanlon, D.O., 2019. The complex defect chemistry of antimony selenide. J. Mater. Chem. 7, 10739.
Sharma, S., Jain, K.K., Sharma, A., 2015. Solar cells: in research and applications—a review. Mater. Sci. Appl. 6, 1145–1155.
Shen, K., Zhang, Y., Wang, X., Ou, C., Guo, F., Zhu, H., Liu, C., Gao, Y., Schropp, R.E.I., Li, Z., Liu, X., Mai, Y., 2020. Efficient and stable planar n–i–p Sb_2Se_3solar cells enabled by oriented 1D trigonal selenium structures. Adv. Sci. 7, 1–10.
Steinmann, V., Brandt, R.E., Buonassisi, T., 2015. Photovoltaics: non-cubic solar cell materials. Nat. Photonics 9, 355–357.
Stoliaroff, A., Lecomte, A., Rubel, O., Jobic, S., Zhang, X.H., Latouche, C., Rocquefelte, X., 2020. Deciphering the role of key defects in Sb_2Se_3, a promising candidate for chalcogenide-based solar cells. ACS Appl. Energy Mater 3, 2496–2509.
Tang, R., Zheng, Z.H., Su, Z.H., Li, X.J., Wei, Y.D., Zhang, X.H., Fu, Y.Q., Luo, J.T., Fan, P., Liang, G.X., 2019. Highly efficient and stable planar heterojunction solar cell based on sputtered and post-selenized Sb_2Se_3 thin film. Nano Energy 64, 103929.
Tyagi, V.V., Rahim, N.A.A., Rahim, N.A., Selvaraj, J.A.L., 2013. Progress in solar PV technology: research and achievement. Renew. Sustain. Energy Rev. 20, 443–461.
Vaidhyanathan, R., Pinjare, S.L., Sobhanadri, J., 1983. The optical properties of $AgInTe_2$ thin films. Thin Solid Films 105, 157–162.
Watahiki, T., Kobayashi, Y., Morioka, T., Nishimura, S., Niinobe, D., Nishimura, K., Tokioka, H., Yamamuka, M., 2016. Analysis of short circuit current loss in rear emitter crystalline Si solar cell. J. Appl. Phys. 119, 204501.
Wu, C.-H., Williams, R., 1983. Limiting efficiencies for multiple energygap quantum devices. J. Appl. Phys. 54, 6721.
Yamaguchi, M., Lee, K.H., Araki, K., Kojima, N., 2018. A review of recent progress in heterogeneous silicon tandem solar cells. J. Phys. D Appl. Phys. 51, 133002.
Yang, J., Fan, Q., Cheng, X., 2017. Prediction for electronic, vibrational and thermoelectric properties of chalcopyrite AgX(X=In,Ga)Te_2: PBE+U approach. R. Soc. Open Sci. 4, 170750.
Yater, J.A., Landis, G.A., Bailey, S.G., Olsen, L.C., Addis, F.W., 1996. ZnSe Window Layers for GaAs Solar Cells, Conference Record of the IEEE Photovoltaic Specialists Conference, pp. 65–68.
Yoo, J.J., Seo, G., Chua, M.R., Park, T.G., Lu, Y., Rotermund, F., Kim, Y.K., Moon, C.S., Jeon, N.J., Correa-Baena, J.P., Bulović, V., Shin, S.S., Bawendi, M.G., Seo, J., 2021. Efficient perovskite solar cells via improved carrier management. Nature 590, 587–593.
Yablonovitch, E., Tiedje, T., Witzke, H., 1982. Meaning of the photovoltaic band gap for amorphous semiconductors. Appl. Phys. Lett. 41, 953–955.
Yoshikawa, K., Kawasaki, H., Yoshida, W., Irie, T., Konishi, K., Nakano, K., Uto, T., Adachi, D., Kanematsu, M., Uzu, H., Yamamoto, K., 2017. Silicon heterojunction solar cell with interdigitated back contacts for a photoconversion efficiency over 26%. Nat. Energy 2, 17032.
Zhou, Y., Wang, L., Chen, S., Qin, S., Liu, X., Chen, J., Xue, D.J., Luo, M., Cao, Y., Cheng, Y., Sargent, E.H., Tang, J., 2015. Thin-film Sb_2Se_3 photovoltaics with oriented one-dimensional ribbons and benign grain boundaries. Nat. Photonics 9, 409–415.